Archives of Civil and Mechanical Engineering (2021) 21:159
https://doi.org/10.1007/s43452-021-00292-6

ORIGINAL ARTICLE

Self-deployable tensegrity structures for adaptive morphing of helium-filled aerostats

Lech Knap[1] · Andrzej Świercz[2] · Cezary Graczykowski[2] · Jan Holnicki-Szulc[2]

Received: 7 February 2021 / Revised: 12 July 2021 / Accepted: 8 August 2021 / Published online: 4 October 2021

Abstract

In this paper, the authors propose, investigate, and discuss a concept of novel type of deployable helium-filled aerostat as a low-cost mean of transport. Internal construction of the aerostat is based on ultra-light tensegrity structure equipped with prestressed tensioned elements of controllable lengths. Such tensegrity structure allows for adaptive morphing of the aerostat understood as simultaneous controllable modifications of aerostat volume and shape during the flight. The controlled volume changes enable influencing buoyancy force and obtaining desired vertical motion during the ascending and descending process. In turn, external shape changes allow for lowering the aerodynamic drag and energy usage needed to uphold stable horizontal position or maintain the desired flight path. Moreover, such internal structure allows for convenient storage, transportation and deployment of the aerostat construction on the ground or in required point at the atmosphere. The article presents an analysis of the exemplary operational mission of the aerostat. The authors introduce the mechanical model capturing interaction of the internal tensegrity structure and aerostat envelope based on the finite-element method, as well as dynamic model allowing for simulation of the aerostat's vertical and horizontal motion influenced by buoyancy and drag forces. Both these models are used to positively verify the feasibility of the proposed concept of deployable tensegrity-based aerostat with adaptive morphing and its efficiency in realization of the assumed flight mission.

Keywords Tensegrity structure · Internal construction · Shape modification · Helium-filled aerostat · Vertical mobility · Horizontal mobility

List of symbols

$A(m_h, \varepsilon_t, h)$	The horizontal cross-section of the aerostat (in the middle plane), [m^2]
c_x	The drag coefficient (dimensionless),
E_m	The Young modulus of the aerostat envelope, [Pa]
E_c, E_g, E_s	The Young modules of the stiff bar, the elastic and stiff tendons, [Pa]
A_v	The circular cross-section area of the valve's nozzle, [m^2]
$g_a(h)$	The gravity at the altitude h, $\left[\frac{m}{s^2}\right]$
h	The altitude of the aerostat, [m]
k	The volumetric stiffness coefficient of the aerostat envelope (determined from numerical test), $\left[\frac{Pa}{m^2}\right]$
l_t, l_t^0	The actual and initial lengths of the stiff tendons, [m]
m_p, m_s, m_t	The payload, the structural mass and the total mass of the aerostat, [kg]
m_{hacc}	The helium mass in the helium accumulator, [kg]
m_h	The helium mass in the aerostat chambers, [kg]
$p_a(h)$	The atmospheric pressure, [Pa]
$p(m_h, \varepsilon_t, h)$	Helium pressure in the aerostat chambers, [Pa]
p_{hacc}	Helium pressure in the accumulator, [Pa]
Q_d, Q_g, Q_b	The drag, gravity, buoyancy force, [N]
q_h	Mass flow rate of helium, $\left[\frac{kg}{s}\right]$
R	Individual gas constant for helium, $\left[\frac{J}{K\,kg}\right]$
$T_a(h)$	The ambient temperature at the altitude h, [K]

✉ Cezary Graczykowski
cgraczyk@ippt.pan.pl

[1] Institute of Vehicles and Construction Machinery, Warsaw University of Technology, Narbutta 84, 02-524 Warsaw, Poland

[2] Institute of Fundamental Technological Research, Polish Academy of Sciences, Pawińskiego 5B, 02-106 Warsaw, Poland

v	The vertical velocity of the aerostat, $\left[\frac{\mathrm{m}}{\mathrm{s}}\right]$
V_0	The design volume of the aerostat, [m^3]
$V(m_\mathrm{h}, \varepsilon_\mathrm{t}, h)$	The operational volume of the aerostat, [m^3]
V_hacc	The volume of the helium accumulator, [m^3]
ε_t	Shortening of the stiff tendons of the tensegrity structure (dimensionless),
κ	The adiabatic exponent for helium (dimensionless),
$\rho_\mathrm{a}(h)$, ρ_hacc	The air density at the altitude and the helium density in the helium accumulator, $\left[\frac{\mathrm{kg}}{\mathrm{m}^3}\right]$
ρ_c, ρ_g, ρ_s	Densities of bars (and stiffening plates), elastic and stiff tendons, $\left[\frac{\mathrm{kg}}{\mathrm{m}^3}\right]$

Subscripts

a	Atmospheric parameter
h	Helium parameter
hacc	Helium accumulator parameter
c	Carbon material properties
g	Elastic tendon properties
s	Stiff tendon properties

1 Introduction

Although airships and balloons were the first air vehicles built by men their application is still very limited. A relatively short episode of their wider use were military applications, which included reconnaissance missions, bombing, combat of submarines and ocean surveillance [1, 2]. But the problems related to construction of safe airships satisfying vertical and horizontal mobility requirements, opposed to the rapid development of aviation, caused the lack of interest in this type of constructions for many years.

However, technological and industrial changes at the beginning of this century, which require cheap acquisition, processing and transmission of information, have caused that many new-generation airships characterized by large safety and the ability to take long-term flights at a given altitude and to transport heavy loads over considerable distances were constructed. Simultaneously, the total costs (mainly consisting of fuel and service) for cargo transport or for exploration of stratosphere, mesosphere—and even space observation—are much lower than in case of using airplanes or satellites [3, 4].

The wider use of all advantages of helium-filled vehicles is provided by airships. Currently constructed airships successfully fulfill various purposes, e.g., provide communication in hardly reachable areas (including ensuring the possibility of using 4G/5G technology), serve as reconnaissance and surveillance systems, military communication centers or research pseudo-satellites [5].

Several project conducted during last 3 decades were oriented towards development of High Altitude Pseudo Satellites (HAPS) operating in the stratosphere, 20–30 km above the sea level, and conducting various types of surveillance and intelligence missions [6]. Such high-altitude aerostats are planned to be constructed as unmanned aircrafts, which are powered by solar energy and may remain in space for more than one year without the need of landing. This class of space vehicles includes stratospheric airplane Zephyr S[1], as well as constant volume airships such as Russian Berkut[2] and French Stratobus[3]. Typically, such airships have very large dimensions including lengths up to 300 m and diameters up to 50 m and their vertical mobility is controlled by changing the mass of the gas filing the main envelope or internal storage tanks. In alternative design of the airship, the volume of the airship significantly changes during the ascending and descending process as a result of internal pressure changes. The example is US construction HiSentinel80, which volume in the stratosphere is about 12–14 times larger than initial volume at the ground level [7].

One of the problems associated with long-term (months-long) floating of aerostats at high altitudes is the helium-tightness of the extremely thin coatings, which are applied because the load capacity of airships largely depends on the self-weight of the structure and their increase reduces the possible payload. During long-term missions substantial helium losses result in the need of helium supplementation, which requires complicated logistics associated with collision-free grounding and lifting of large, volume-changing object to the stratosphere. The additional problems are related to heating of the aerostat coating (and internal helium) during the day and its cooling at the night. These temperature changes have to be compensated by change of the buoyancy force in order to maintain stable assumed height of the aerostat. Another problem is undesirable horizontal movement of the aerostat caused by lateral gusts [8], which have different directions and various speeds depending on altitudes[4,5] and have to be compensated by propulsion systems, significantly reducing aerostat's load capacity.

[1] More information at the webpage (accessed 2021 Jan 18): https://www.airbus.com/defence/uav/zephyr.html.

[2] Manufacturer's website (accessed 2021 Jan 18): http://rosaerosystems.com/projects/obj687.

[3] More data at webpage (accessed 2021 Jan 18): https://www.thalesgroup.com/en/worldwide/space/news/whats-stratobus

[4] The average winds data can be found at webpage (accessed 2021 Jan 18): http://prismaticltd.co.uk/products/phast.

[5] Overview of programs funded within the Department of Defense (USA) can be found at webpage (accessed 2021 Jan 18): https://apps.dtic.mil/dtic/tr/fulltext/u2/a568211.pdf.

The important research topic related to the aerostats design is the mechanical resistance for alternating environmental conditions and modeling the dynamic behavior during their flight. Aerostats aerodynamics can be simulated using modern computational techniques including application of fluid–structure interaction approach, which allows to capture the influence of the flow on airship deformation and vice versa [9]. The detailed analysis of deformation of aerostat envelope including its compression and wrinkling can be modeled using membrane theories implemented in finite-element method [10]. The diurnal temperature difference for long-endurance station-keeping performance is proposed in [11]. This work deals with the thermal model of the envelope, internal gas including simulation of velocity field, computational model and adjustment of the diurnal temperature difference. The paper [12] presents modal characteristics of a flexible airship envelope made of Uretek 3216LV and includes dry and wet modal analysis. In addition, the pressure difference, the geometric dimension, the welding seam were considered as factors affecting the modal analysis results of the airship hull. An experimental approach to the study of spherical membranes subjected to concentrated loads focused on wrinkling patterns is presented in [13]. In [14], the mechanical models for large deformations of the membrane are investigated using membrane and shell elements. The authors discussed and emphasized the importance of the pressure perturbations and boundary conditions. They recommend the membrane model to simulate the membrane deformations.

An efficient methods for modeling of the dynamics of flexible airships are based on combination of flight dynamics, structural dynamics and aerodynamics [15, 16]. General advantages of the optimization of the trajectory of airship flight are described in [17]. The methods applied for control of airship trajectories include a guidance-based path-following control [18], universal stabilizing feedback leading to robust control laws [19], minimum-time and minimum-energy optimal control [20], adaptive control laws, e.g., with feedback linearization [21] or redundant control systems including position tracking, velocity regulator and altitude stabilization [22].

The entirely novel, proposed by the authors, construction of the helium aerostat is based on application of specially designed, controllable tensegrity structure [23, 24] equipped with active tendons. The previous research in the field of tensegrity structures concerned both the classical [25, 26] and the controllable [27] structures, and was aimed at development of form-finding methods, control algorithms and applications limited mainly to civil engineering. In particular, the procedure for form-finding of tensegrity structures was studied in [14], while another approach extended to hyperelastic tensegrity structures based on strut finite elements and unconstrained nonlinear programming was shown in [28]. The problems of tensegrity forms control were also considered by researchers in the case of simple planar [29], spatial [30, 31] structures or footbridges [32]. It has to be emphasized that application of controllable tensegrity structures as a supporting structure of the aerostat was not proposed in the subject literature so far.

The objective of this paper is introduction and initial investigation of the concept of using controllable ultra-light, rod-cable internal tensegrity structure with active tendons for supporting aerostat coating. Such approach is proved to have several significant advantages. At the first, control of tendons lengths enables change of the aerostat volume, which affects actual buoyancy force, aerostat equilibrium altitude and enables obtaining desired vertical mobility (V-mobility). Second, control of active tendons allows for structural shape control performed in order to minimize aerodynamic wind drifts and maintain aerostat horizontal stability (H-stability). The combination of V-mobility and H-stability is further called adaptive morphing. Generally, the process of adaptive morphing, as demonstrated, e.g., in [33], covers continuous transition of aerostat shape in a controlled way to provide a precise position control, independently on the operational conditions. Another application of adaptive morphing is reduction of energy consumption required to keep the aerostat in a determined position under actual atmospheric conditions. Thirdly, it enables aerostat transportation and self-deployment into a stable 3D configuration at selected point of the atmosphere.

The contribution of the paper is development of the numerical models and conducting numerical simulations which prove the feasibility of above presented concept of tensegrity-based aerostat and the paradigm of adaptive morphing. In particular, simulations conducted using numerical model of vertical motion of the aerostat, which take into account buoyancy and aerodynamic forces obtained from FSI analysis, show the possibility of obtaining the desired vertical path of the aerostat. Moreover, the detailed finite-element model of the aerostat with internal tensegrity structure reveals the influence of internal pressure and change of tendons lengths on aerostat deformation and generated internal forces. Both types of conducted simulations prove that the proposed concept is an appealing solution and can be potentially applied in practice.

The paper is organized as follows: in Sect. 2, the authors present the concept of deployable aerostat internally supported by adaptive tensegrity structures. Next, in Sect. 3, the mathematical model of vertical mobility based on

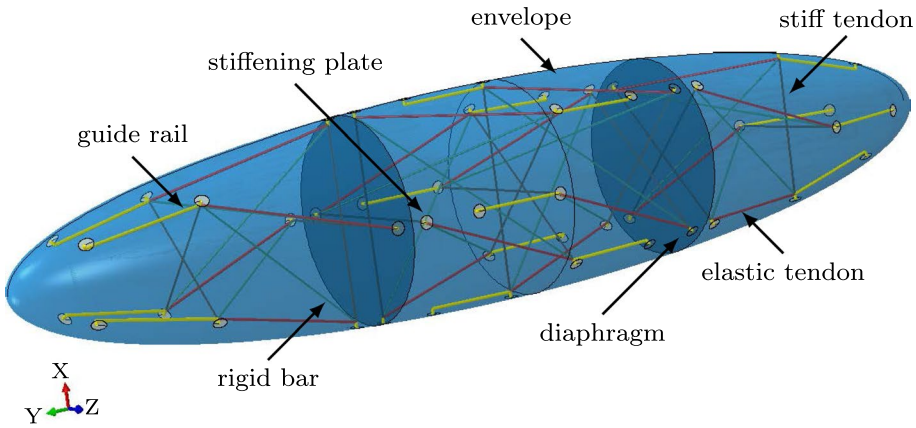

Fig. 1 Scheme of the proposed aerostat

analytical description of atmospheric parameter variations and aerodynamic forces is introduced. In Sect. 4, numerical model of aerostat mobility prepared using Matlab/Simulink and detailed model of aerostat construction developed in the Abaqus software are presented. The models are used for simulation of aerostat behavior under atmospheric conditions, structural assessment and adaptive morphing to control an aerostat altitude. Finally, in Sect. 5, the obtained results, which fully confirm the feasibility of the proposed tensegrity-based aerostat and the concept of adaptive morphing, are summarized.

2 Design of the helium aerostat

The proposed Adaptive Helium Aerostat with the Self-Deployable Tensegrity (AHA-SDT) is presented in Fig. 1. The designed external shape of the envelope is based on an ellipsoid with a circular cross-section in the vertical plane. The length of the major axis is equal to 10 m, whereas the minor axes have the lengths of 2 m. The internal space is divided into three chambers by means of the two circular diaphragms distanced by 3.34 m and symmetrically arranged with respect to the vertical middle plane. Unlike the classical tensegrity or cable-driven control trusses, the proposed design of the aerostat internal structure utilizes two types of tendons: elastic and stiff tendons. The elastic tendons remain passive but can be significantly deformed, while stiff tendons lengths can be controlled during aerostat motion. The propose internal construction provides significant advantages both for the case of aerostat transportation and adaptation to actual flight conditions.

The possibility of significant deformations of the elastic tendons, after removing helium from the balloon, enables transformation of the aerostat into a compact form (an unstable 1D configuration) and its placement in a container. This approach facilitates the aerostat transportation and self-deployment into a stable 3D configuration (including simultaneously the fast helium inflation) at a precisely planned point of the atmosphere. An airplane, airship or launch rocket can be used for lifting up the container with compact form of the aerostat.

In turn, controlled changes of stiff tendons lengths combined with changes of internal pressure enable the process of adaptive morphing including control of the actual volume of the aerostat affecting generated buoyancy force and its vertical mobility (V-mobility) as well as changes of aerostat shape affecting generated drag forces and its horizontal stability (H-stability). The above process of adaptive morphing can be efficiently performed using controllable devices (retractors, i.e., rotary electric motors or linear actuators) for contraction or elongation of stiff tendons. This leads to the redistribution of internal forces in the envelope and supporting structure usually including a large configuration change of the aerostat.

An additional advantage of the proposed Adaptive Helium Aerostat with the Self-Deployable Tensegrity (AHA-SDT) structure is possibility of applying concentrated forces coming from a payload (in the nodal points of the SDT internal structure) to the ellipsoidal envelope of the aerostat.

The external envelope is supported by four modules of tensegrity-based structures: one module in each the outermost chambers and two modules in the middle chamber. A single module of the tensegrity structure consists of four rigid bars, four elastic tendons and eight stiff tendons whose space arrangement is shown in Fig. 2.

The Young modulus of the stiff tendons is assumed to be higher a few orders of magnitude in comparison to the elastic counterparts. In the proposed structure, the tensegrity module is square-based and formed from the stiff tendons (form two crosses) and rotated by an angle of 45° to each other. Retractors, located at the center of crosses, control the length of each stiff tendon, depending on the applied control strategy. An application of elastic tendons makes possible (utilizing external forces) to fold the modules together with the envelope and diaphragms into the compact and

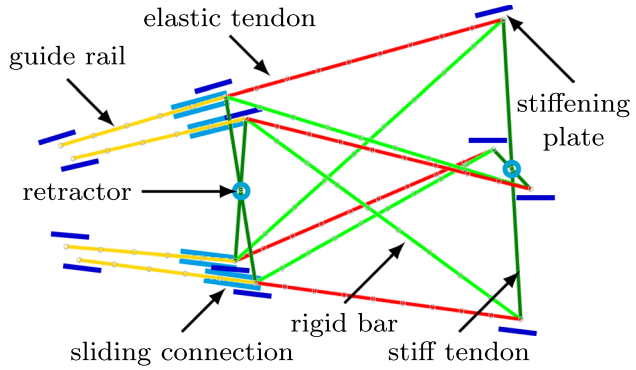

Fig. 2 Scheme of the single module of the tensegrity structure with guide rails

transportable form. On one side, the nodes of the module are pin-jointed to the stiffening plates embedded into the envelope, and slidably or pin-joined (switchable fashion) to the guide rails on the other. When sliding connection is activated (e.g., preparation for transportation), the movable joints are free to move in some limited regime. At both ends, the guide rails are connected to the stiffening plates.

A control of the aerostat volume V and shape at altitude h can be achieved in two ways using retractors based on electric motors: by modifying the length of stiff tendons or elastic tendons. For the given mass of helium m_h in the aerostat, this approach leads to the perturbation of internal pressure p. In such control model, the shortening of stiff tendons reduces the aerostat volume V and the buoyancy force Q_b resulting in the reduction of the aerostat altitude h.

Similarly, a reduction of the helium mass m_h inside the aerostat causes drop of the internal pressure p and partial folding of the tensegrity structure. This also yields a reduction of the aerostat volume V. Control of the tendons lengths and helium mass m_h inside the aerostat enables obtaining desired altitude h. The aerostat can be optionally equipped with an ultra-light compressor and an additional small helium accumulator, which enable precise control of internal pressure p and resulting volume V and aerostat altitude h.

3 Mathematical model of vertical mobility

In this article, we focus on the vertical movement of the aerostat, i.e., V-mobility. Initially, the aerostat is tethered at the ground level $h(0) = h_0$ (in general $h(0) > h_0$) and inflated with the use of an external helium pressure accumulator (helium tank). The tank has a volume of V_{hacc}, an initial pressure of $p_{hacc}(0)$ and the final overpressure of Δp_{hacc}. If the tank final overpressure Δp_{hacc} is reached, the valve closes and the flow of helium is stopped. After that, the main pneumatic accumulator is disconnected. If the mass of the helium inside the aerostat is appropriate, the untethered structure starts to ascend.

In the analytical model, we assume that helium pressure p in the aerostat is equal to atmospheric pressure p_a when the aerostat volume $V < V_0$. In turn, when the aerostat is inflated to volume greater than the design volume, i.e., $V > V_0$, the internal pressure p increases above the atmospheric one, i.e., $p > p_a$ and the aerostat envelope expands elastically. Thanks to this, more precise control of the aerostat altitude during the ascending and descending process is possible. On the other hand, maintaining overpressure $\Delta p = p - p_a$ inside the aerostat also prevents the aerostat from rising excessively high and provides some resistance to lateral gusts. The value of the volumetric stiffness coefficient k of the envelope is determined experimentally or based on numerical analysis. In the presented approach, a finite-element analysis was performed using the Abaqus package to assess the parameter k. More details are presented in Sect. 4.

The developed analytical model for the aerostat utilizes the following assumptions:

- The designed volume of the aerostat is equal to V_0;
- Total mass of the aerostat structure m_s contains the supporting structure, the aerostat envelope and diaphragms;
- Mass of the lifting helium $m_h(t)$ is time-dependent. The compressor and controlled valve installed in the small tank allow for the helium flow management in the aerostat chambers;
- A helium mass inside the aerostat at the initial state is equals to $m_h(0)$;
- A payload m_p includes the ultra-light helium compressor with a small tank, micro-electronics, micro-mechanical devices, etc.;
- The total mass of the aerostat is m_t and contains mass of aerostat structure, the total mass of helium and the payload;
- After the designed mass of helium is inflated into the aerostat chambers, the main helium pressure accumulator is disconnected and remains on the ground;
- When the valves installed in the diaphragms remain open, the helium pressures in all chambers are equal. The special case with closed valves is analyzed in Sect. 4.3;
- The volumetric stiffness coefficient k of the aerostat structure is determined in a numerical test and valid for $V > V_0$;
- The elongation of the stiff tendons ε_t can be only applied for $V < V_0$ and unchanged helium mass $m_h = \text{const}$.

The values of atmosphere parameters depend on the altitude h, such as temperature T_a, pressure p_a, gravity g_a and density

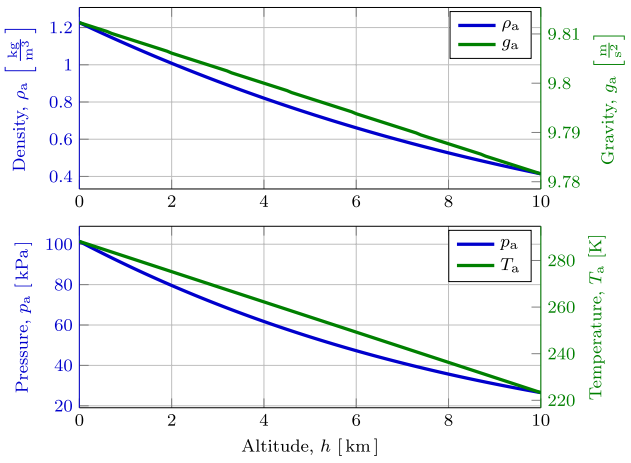

Fig. 3 Atmosphere parameters according to the NASA model

ρ_a, were assumed using the Earth atmosphere model[6]. These parameters are presented in Fig. 3.

During analysis of the vertical movement of the aerostat it is necessary to determine the values of the following forces acting on the aerostat:

(I) the weight of the aerostat:

$$Q_g(h) = m_t\, g_a(h), \tag{1}$$

(II) the buoyancy force:

$$Q_b(m_h, \varepsilon_t, h) = \rho_a(h)\, g_a(h)\, V(m_h, \varepsilon_t, h), \tag{2}$$

(III) the aerodynamic drag force:

$$Q_d(m_h, \varepsilon_t, h) = \mathrm{sgn}(v)\, c_x(v)\, \rho_a(h)\, A(m_h, \varepsilon_t, h)\, \frac{v^2}{2}, \tag{3}$$

where v is the vertical velocity of the aerostat, $A(m_h, \varepsilon_t, h)$ the horizontal cross-section area (in the middle plane) of the aerostat and $\varepsilon_t = \frac{l_t - l_t^0}{l_t^0}$ denotes the elongation of the stiff tendons with the actual length l_t and the initial length l_t^0. The values of the aerodynamic drag coefficient c_x can be determined numerically or experimentally.

The relationships given by Eqs. (1)–(3) allow for the formulation of the equation of vertical motion of the aerostat in the following form:

$$m_t \frac{d^2h}{dt^2} = -Q_g + Q_b - Q_d. \tag{4}$$

[6] The model is available at NASA's web page (accessed 2021 Jan 18):
https://www.grc.nasa.gov/www/K-12/airplane/atmosmet.html.

Equation (4) enables determination of the vertical acceleration $a(t) = \frac{d^2h}{dt^2}$, velocity $v(t) = \frac{dh}{dt}$ and actual height $h(t)$ of the aerostat. When the aerostat begins to ascend from the ground level h_0, the calculation of volume V and pressure p for the actual aerostat altitude h is based on the determination of the new values of parameters $p_a(h)$, $g_a(h)$, $\rho_a(h)$, $T_a(h)$ for the actual altitude $h(t)$.

The vertical motion of the aerostat can be controlled by changing its actual volume V, which significantly influences the buoyancy force Q_b. According to the proposed concept of adaptive tensegrity-based aerostats, the control of aerostat volume V can be conducted in two manners:

- Helium mass control—by changing actual mass of helium m_h inside the aerostat,
- Tendons length control—by changing actual length of the tendons of tensegrity structure supporting envelope of the aerostat (introducing their shortening ε_t).

The control of the helium mass inside the aerostat has different effect when actual volume of the aerostat V is smaller and larger than the design volume V_0. In the former case, the pressure inside the aerostat equals to atmospheric pressure at the actual altitude h:

$$p = p_a(h) \quad \text{for} \quad V \le V_0. \tag{5}$$

In the latter case, the actual volume of the aerostat depends on the actual difference of internal and external pressure according to the formula:

$$V = V_0 + \frac{1}{k}\, V_0 \big(p - p_a(h)\big) \quad \text{for} \quad V > V_0, \tag{6}$$

where k is the volumetric stiffness coefficient defining global expansion of the aerostat volume, which can be determined either from experiments or analysis based on Finite-Element Method. In turn, in case of control of tendons lengths the actual volume of the aerostat V depends on both actual tendons shortening ε_t and actual difference of internal and external pressure. Such dependence assumes general form:

$$V = V\big(\varepsilon_t, p - p_a(h)\big) \tag{7}$$

and cannot be defined a priori in a form of closed analytical formula. Since Eqs. (5)–(7) include unknown value of pressure p, they have to be combined with ideal gas law:

$$p\, V = m_h\, R\, T_a(h). \tag{8}$$

Equations (5)–(8) constitute a closed system of equations which allows to find dependence of volume V (and pressure p) on control variables m_h and ε_t.

The solution of the above system of equations is conducted as follows. Introducing Eq. (5) into Eq. (8) directly yields dependence of volume V on helium mass m_h for the

case $V \le V_0$. In turn, combining Eqs. (6) and (8) leads to quadratic equation with respect to V:

$$\frac{k}{V_0}V^2 + \left(p_\mathrm{a} - k\right)V - m_\mathrm{h} R T_\mathrm{a} = 0, \tag{9}$$

which has two solutions:

$$V = \frac{V_0}{2k}\left(k - p_\mathrm{a} - \sqrt{\Delta}\right), \tag{10a}$$

$$V = \frac{V_0}{2k}\left(k - p_\mathrm{a} + \sqrt{\Delta}\right), \tag{10b}$$

with a determinant:

$$\Delta = \left(p_\mathrm{a} - k\right)^2 + 4k\,\frac{m_\mathrm{h} R T_\mathrm{a}}{V_0}. \tag{11}$$

Due to positive values of all thermodynamic quantities in the second term of the definition of determinant Δ, the value of determinant satisfies $\Delta > (p_\mathrm{a} - k)^2$, which implies the inequality $\sqrt{\Delta} > |p_\mathrm{a} - k|$. Thus, only one solution given by Eq. (10b) satisfies the physical condition $V > 0$ and will be incorporated into the further considerations. Finally, general dependence given by Eq. (7) can be determined using either experimental data or simulations based on Finite-Element Method and approximated as an analytical function. Then, introducing pressure p determined from Eq. (8) allows to rewrite Eq. (7) in the form:

$$V = \widetilde{V}(\varepsilon_\mathrm{t}, m_\mathrm{h}, h), \tag{12}$$

which indicates dependence of volume on tendons shortening, helium mass and the actual altitude of the aerostat. In a special case of quasi-static motion of the aerostat, the actual altitude can be determined from the static equilibrium condition resulting from Eq. (4) and it depends on actual aerostat volume: $h = h(V)$. Thus, Eq. (12) can be rewritten as follows:

$$V = \hat{V}(\varepsilon_\mathrm{t}, m_\mathrm{h}). \tag{13}$$

Eventually, the dependence of the actual volume of the aerostat on control variables ε_t and m_h can be written in the following form:

$$V = \begin{cases} \frac{m_h R T_a(h)}{p_a(h)} & \text{for } V \le V_0 \text{ and } \varepsilon_t = 0, \quad (14a) \\ \frac{V_0}{2k}\left(k - p_a + \sqrt{\Delta}\right) & \text{for } V > V_0 \text{ and } \varepsilon_t = 0, \quad (14b) \\ \tilde{V}\left(\varepsilon_t, m_h, h\right) & \text{for } \varepsilon_t \neq 0, \quad (14c) \end{cases}$$

The above formulae can be directly introduced into equation of motion of the aerostat (Eq. (4)) which is solved to find change of aerostat volume being the result of applied control.

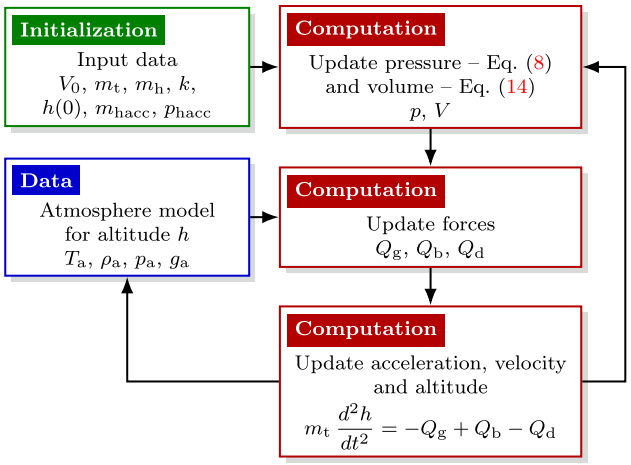

Fig. 4 Block diagram for the pressure and volume computation

The knowledge of the volume V enables determination of forces Q_g, Q_b, Q_d acting on the aerostat from Eqs. (1)–(3) and computation of the aerostat kinematics in accordance with Eq. (4). The block diagram utilized for the numerical computation of the aerostat V-mobility is presented in Fig. 4.

Notes on the initial inflation: As already mentioned, the elaborated mathematical model covers also the initial process of the aerostat inflation. Here, we assume that the aerostat inflation takes place on the ground level h_0. The computation of the helium mass m_h and helium pressure p during the inflation is based on the gas flow equations taking into account the conditions of subcritical and critical (choked) flow. The remaining assumptions are:

- The cross-section area of the valve's nozzle A_v;
- The coefficient $\beta_{\mathrm{cr}} = \left(\frac{2}{\kappa+1}\right)^{\frac{\kappa}{\kappa-1}}$, where $\kappa = c_\mathrm{v}/c_\mathrm{p}$ is the adiabatic exponent;
- The coefficient $\beta = p/p_\mathrm{hacc}$;
- The mass flow rate q_h for $\beta \le \beta_{\mathrm{cr}}$:

$$q_\mathrm{h} = A_\mathrm{v}\sqrt{\kappa\, p_\mathrm{hacc}\,\rho_\mathrm{hacc}\left(\frac{2}{\kappa+1}\right)^{\frac{\kappa+1}{\kappa-1}}}, \tag{15}$$

  where $\rho_\mathrm{hacc} = m_\mathrm{hacc}/V_\mathrm{hacc}$ and m_hacc indicates helium mass remaining in the main helium pressure accumulator;
- The mass flow rate q_h for $\beta > \beta_{\mathrm{cr}}$:

$$q_\mathrm{h} = A_\mathrm{v}\sqrt{\frac{2\kappa}{\kappa-1}\,p_\mathrm{hacc}\,\rho_\mathrm{hacc}\left(\beta^{\frac{2}{\kappa}} - \beta^{\frac{\kappa+1}{\kappa}}\right)}; \tag{16}$$

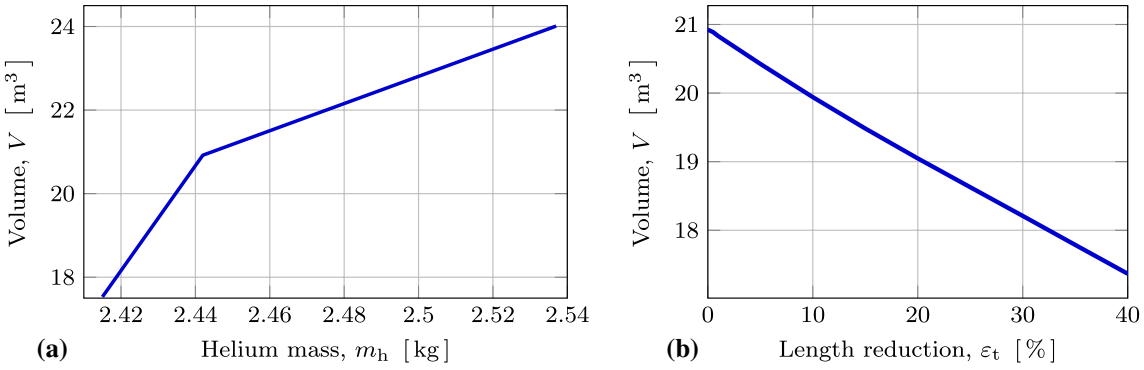

Fig. 5 Aerostat volume change: **a** in a function of the pressure difference inside and outside, **b** caused by uniform length reduction of tendons

– The helium mass m_{hacc} remaining in the main helium pressure accumulator:

$$m_{\mathrm{hacc}} = m_{\mathrm{hacc}}(0) - \int_{\tau_1}^{\tau_2} q_{\mathrm{h}}\, dt, \tag{17}$$

where τ_1 and τ_2 determine the analyzed period;

– The helium mass m_{h} in the aerostat's chambers:

$$m_{\mathrm{h}} = m_{\mathrm{h}}(0) + \int_{\tau_1}^{\tau_2} q_{\mathrm{h}}\, dt; \tag{18}$$

– The volume V of the aerostat:

$$V = \frac{m_{\mathrm{h}} R\, T_{\mathrm{a}}(0)}{p_{\mathrm{a}}(0)}; \tag{19}$$

– The pressure p_{hacc} in the main helium accumulator:

$$p_{\mathrm{hacc}} = \frac{m_{\mathrm{hacc}} R\, T_{\mathrm{a}}(0)}{V_{\mathrm{hacc}}}. \tag{20}$$

The computation of the initial helium inflation is important for the required time assessment as well as the designing the mass and volume of the pressure accumulator. This is crucial for missions starting from altitude $h_0 > 0$.

4 Numerical models of the aerostat

In this part, the numerical results of the aerostat introduced in previous sections are presented. To this end, the Simulink/Matlab and Abaqus packages are complementary employed. While the Simulink/Matlab code is focused on the aerostat's mission path (kinematics with pressure and volume computations), the Abaqus model is used mainly for the internal forces assessment of the structure in some selected time points. In the latter case, the aerostat was loaded quasi-statically by an external pressure corresponding to the altitude determined in Simulink/Matlab. On the other hand, the numerical model delivers to the Simulink/Matlab procedures the volumetric stiffness coefficient k and the dependency of volume V and the length reduction of tendons ε_{t}. The aerostat volume can be controlled by changing helium mass m_{h} and by shortening of tendons ε_{t}. The dependence of aerostat volume on required helium mass resulting from Eqs. (14a) to (14b) is presented in Fig. 5a. The control of aerostat volume V by changing actual tendons lengths was conducted exclusively for aerostat volume smaller than the design volume V_0. The reason for this limitation is that in the case of aerostat volume V larger than the design volume V_0, the shortening of tendons typically causes excessive stresses in the aerostat envelope. The dependence of actual volume of the aerostat on actual shortening of the tendons ε_{t} was computed using Finite-Element Analysis of aerostat structure and by assuming given helium mass m_h, for which the process of adaptive morphing was conducted. The simulation revealed approximately linear dependence between actual uniform shortening of all tendons ε_{t} and actual volume V of the aerostat, see Fig. 5b. One should be aware that although Fig. 5 shows the mentioned relationships, the aerostat volume refers to the atmospheric conditions at a given altitude obtained in the analyzed scenarios.

Generally, the aerostat mission is planned in the following way: inflation of the designed mass of helium into the aerostat chambers, then raising up the aerostat from the ground level h_0 to the operational altitude h_2, after that a reduction of the operational altitude to $h_1 < h_2$, and finally landing phase with a touchdown (reaching h_0). Before the landing phase, there is also investigated an intermediate aerostat altitude h_{s}, (which could be used to facilitate its servicing from an air-hot balloon). A change of the aerostat altitude to h_{s} is considered in two variants:

– Variant I: descent controlled by a compression of a small portion of helium (just a continuation of helium mass control strategy), and

Table 1 Values of parameters assumed in the analysis performed using Matlab/Simulink

$m_t = 17.709$ kg	$m_h^{II}(0) = 2.347$ kg	$h_s = 1\,978$ m	$R = 2079.3\,\mathrm{J/(K \cdot kg)}$
$m_s = 11.222$ kg	$m_h^{I}(0) = 2.396$ kg	$V_0 = 20.915\,\mathrm{m}^3$	$c_v = 3150.1\,\mathrm{J/(K \cdot kg)}$
$m_p = 3.950$ kg	$m_h(0) = 0$ kg	$p_{hacc}(0) = 300$ bar	$c_p = 5229.4\,\mathrm{J/(K \cdot kg)}$
$m_h(h_2) = 2.537$ kg	$h_1 = 3\,724$ m	$V_{hacc} = 51\,\mathrm{dm}^3$	$k = 14\,206\,\mathrm{N/m}^2$
$m_h(h_1) = 2.442$ kg	$h_2 = 5\,001$ m	$A_v = 9.53 \cdot 10^{-4}\,\mathrm{cm}^2$	$\kappa = 1.66$

– Variant II: descent controlled by a length reduction of tendons (resulting in the volume reduction).

Then, the landing phase (from h_s to h_0) in both variants takes place using helium mass compression. The aerostat mission including variant I and II is investigated in both Simulink/Matlab and Abaqus packages. The computational details and assumptions are presented in the following subsections.

4.1 Vertical mobility analysis in Matlab/Simulink

The analysis of the vertical motion of the aerostat was performed using numerical model developed in Matlab/Simulink software. We assume, the planned aerostat mission covers two operational pre-designed altitudes: $\widetilde{h}_2 = 5.0$ km and $\widetilde{h}_1 = 3.7$ km and the optional servicing altitude of $\widetilde{h}_s = 2.0$ km. The symbols $\widetilde{h}_1$ and $\widetilde{h}_2$ denotes pre-design altitudes, whereas the quantities h_1 and h_2 are the computed altitudes. The implemented aerostat mission consists of the following stages:

(a) An inflation of the initially tethered aerostat using the pre-computed mass of helium by means of the main pressure accumulator at the ground level h_0 ($V < V_0$, cf. paragraph *Notes on the initial inflation* in Sect. 3);
(b) Untethering and ascending of the aerostat to the altitude of h_2 and maintaining this altitude for some time period ($V > V_0$);
(c) Descending of the aerostat to the altitude of h_1 by transferring some amount of helium mass into the additional small tank, such that $V \approx V_0$ and maintaining this altitude for some time period;
(d) Descending of the aerostat from h_1 until touchdown with the intermediate servicing altitude h_s. This is done in two variants: by decreasing of the lifting helium mass (variant I) or applying adaptive morphing (variant II—using a length reduction of stiff tendons). While the aerostat touchdown, helium masses are denoted by $m_h^{I}(0)$ for the variant I and by $m_h^{II}(0)$ for the variant II (see Table 1 for details).

Assuming the payload m_p and the aerostat mass of m_s, the calculated helium mass to be inflated is equal to m_{h2} to reach the pre-designed altitude of $\widetilde{h}_2$. These values and the others indispensable for the lifting path computation are gathered in Table 1. The structural mass m_s of the aerostat was computed based on the finite-element model discussed in Sect. 4.2.

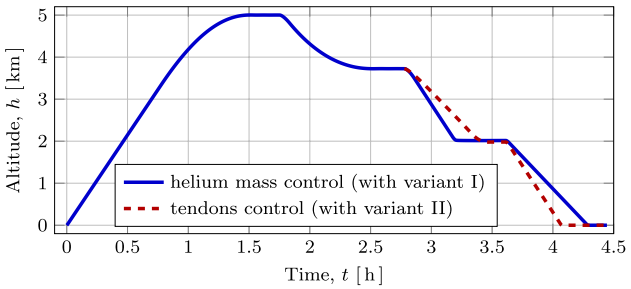

Fig. 6 The aerostat altitude $h(t)$ during its mission computed in Simulink/Matlab

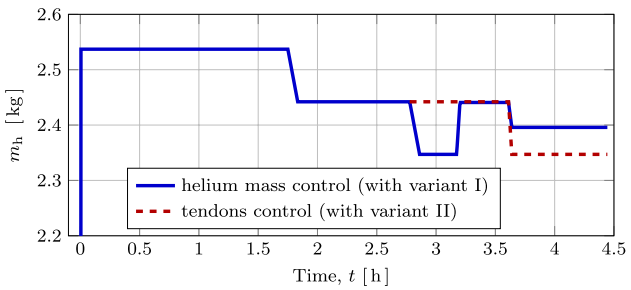

Fig. 7 Lifting mass of helium $m_h(t)$ during the aerostat mission obtained in Simulink/Matlab

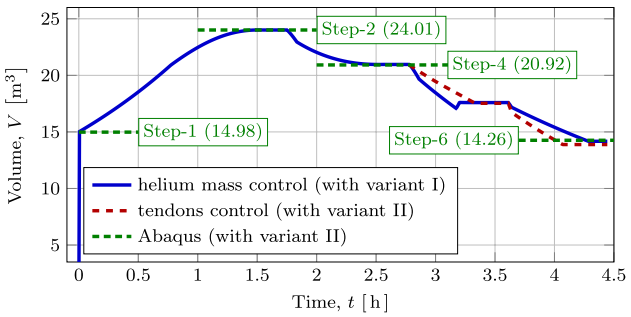

Fig. 8 The aerostat volume $V(t)$ during its mission computed using Matlab/Simulink (blue line) and the Abaqus package (green line, quasi-static process discussed in Sect. 4.2)

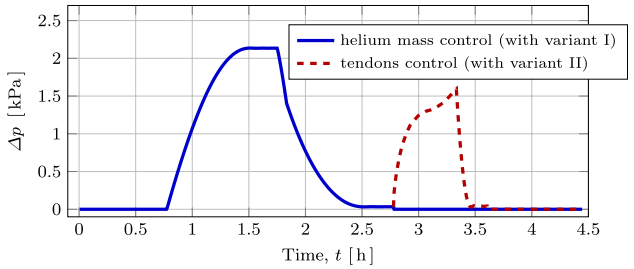

Fig. 9 Pressure difference $\Delta p(h)$ during its mission computed using Matlab/Simulink

The obtained results for helium mass control are presented by blue lines in Figs. 6, 7, 8, 9. The computed time-dependent aerostat mission path $h(t)$ is shown in Fig. 6. The operational altitude h_2 (exact value: 5001 m) is reached after $1\frac{1}{2}$ hours and maintained for the next $\frac{1}{4}$ hour. After that, a small portion of helium is compressed into the small tank and the mass m_{h1} remains in aerostat chambers. This causes the operational altitude reduction to h_1 within approximately $\frac{3}{4}$ hour and further the mission is continued at this altitude for the next $\frac{1}{4}$ hour. Faster altitude change is possible, but requires increased mass variation and such approach is more energy-consuming as demonstrated in [32]. From this point the variant I starts (from h_1 to h_{s}), thus a very small portion of helium should be transferred into the tank. However, to speed up the aerostat descending, firstly excessive mass of helium is compressed (95 grams) and then released into the chambers (93.8 grams) just before the target altitude of h_{s}, which is clearly visible in Fig. 7. This servicing altitude h_{s} is maintained for one hour. Finally, the last portion of helium is transferred into the tank (the remaining mass is $m_{\mathrm{h}}^{\mathrm{I}}(0)$) and after next 1 h, the aerostat lands on the ground. Figures 8 and 9 show the corresponding volume $V(t)$ and pressure difference Δp during the mission.

The alternative results for lowering the aerostat from the altitude h_1 to h_{s} tendons control are also shown in Figs. 6, 7, 8, 9 but are marked by dashed red lines. In contrast to the helium mass control case, the activated electric motors installed at the intersections of stiff tendons cause their smooth and uniform shortening. At the altitude h_{s} the length reduction of each stiff tendon is equal to 34.4%. This causes the aerostat volume decrease and the helium pressure increase in the aerostat chambers as shown in Figs. 8 and 9, respectively. Other scenarios of the stiff tendons shortening are also possible, leading to the different aerostat shapes. Such shape transformations may be important due to horizontal mobility (H-mobility) in various wind conditions.

4.2 Aerostat strength assessment

The aim of the structural analysis of the aerostat during its mission is the assessment of internal forces in the envelope and supporting structure. This objective is obtained using the Abaqus package with the application of the quasi-static loadings. In the initial configuration with a zero-stress state in the envelope, the aerostat is inflated to atmospheric pressure and occupies volume V_0. First, the elastic tendons are pretensioned to level of σ_0, which perturbs negligibly the initial volume V_0. In the next step, helium is partially removed leaving the same amount of mass m_{h2} as listed in Table 1. At the ground level, the same reference atmospheric pressure $p_{\mathrm{a}}(0)$ is assumed acting inside and outside the aerostat. When the aerostat is lifting up, the reference atmospheric pressure $p_{\mathrm{a}}(0)$ remains constant independently on the altitude h, however, the external altitude-dependent compensating pressure $p_{\mathrm{e}}(h)$ is outwardly applied to the aerostat envelope in order to obtain the same loading conditions of the aerostat as determined in the previous subsection:

$$p_{\mathrm{e}}(h) = p_{\mathrm{a}}(0) - p_{\mathrm{a}}(h). \tag{21}$$

The compensating external pressure $p_{\mathrm{e}}(h)$ accompanying the altitude change and gas temperature transition are determined using the atmosphere model (cf. Fig. 3).

For computation purposes, temperature-independent structural materials were assumed, namely:

- A hypothetical aerostat envelope, fabric similar to Antrix (see [34]), with the thickness of t_{m}, the density of ρ_{m}, the Young modulus of E_{m}. It is used to make external envelope and both diaphragms. The total volume of the aerostat in the nominal state is equal to V_0 (middle chamber: V_0^{a} and lateral chambers: $V_0^{\mathrm{b}} = V_0^{\mathrm{c}}$, see Table 2);
- Carbon fiber (the density ρ_{c}, the Young modulus E_{c}). It is used to make rigid bars and guide rails (both element groups with a pipe cross-section with the thickness of t_{c} and the diameter of ϕ_{c}) and the stiffening plates (joining

Table 2 Values of parameters assumed in the analysis using the Abaqus package

$T(0) = 288.2$ K	$\rho_{\mathrm{c}} = 1580\,\mathrm{kg/m^3}$	$\phi_{\mathrm{c}} = 12$ mm	$E_{\mathrm{c}} = 87.0$ GPa
$T(h_1) = 264.1$ K	$\rho_{\mathrm{g}} = 900\,\mathrm{kg/m^3}$	$\phi_{\mathrm{g}} = 3.6$ mm	$E_{\mathrm{g}} = 0.05$ GPa
$T(h_2) = 255.7$ K	$\rho_{\mathrm{m}} = 1390\,\mathrm{kg/m^3}$	$\phi_{\mathrm{p}} = 120$ mm	$E_{\mathrm{m}} = 0.43$ GPa
$T(h_{\mathrm{s}}) = 275.4$ K	$\rho_{\mathrm{s}} = 7850\,\mathrm{kg/m^3}$	$\phi_{\mathrm{s}} = 3$ mm	$E_{\mathrm{s}} = 210.0$ GPa
$t_{\mathrm{c}} = 1$ mm	$h_{\mathrm{s}} = 1\,978$ m	$V_0^{\mathrm{a}} = 10.093\,\mathrm{m^3}$	$\sigma_0 = 2.0$ MPa
$t_{\mathrm{m}} = 50\ \mu$m	$V_{\mathrm{s}} = 17.527\,\mathrm{m^3}$	$V_0^{\mathrm{b}} = 5.411\,\mathrm{m^3}$	

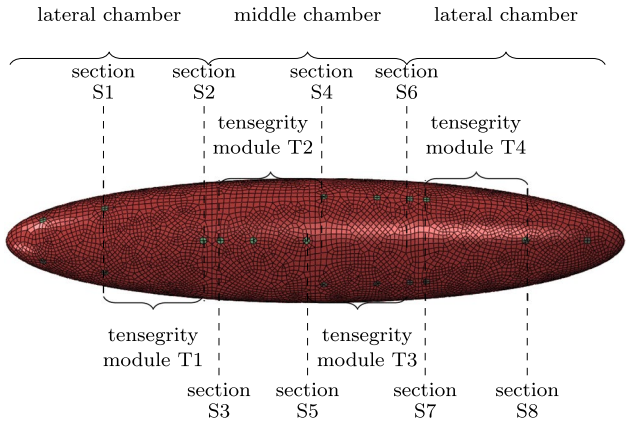

Fig. 10 General view of the numerical model of the aerostat in the initial configuration with marked location of tensegrity modules T1–T4 and aerostat cross-sections S1–S8 containing stiff tendons

construction nodes and envelope) with the diameter of ϕ_p and thickness of t_c;
- Elastic rubber-like material for the tendons (the density ρ_g, the Young modulus of E_g and diameter of ϕ_g). The initial stress imposed in each on those elements is equal to σ_0;
- Steel (the density ρ_s, the Young modulus E_s and diameter of ϕ_s). It is used to make tensioned-only stiff tendons.

The material parameters and geometric data used in the model definition are summarized in Table 2. The values of parameters presented in Table 1 are also valid in this subsection.

The created mesh contains following finite elements:

- Membrane elements (aerostat envelope and diaphragms),
- Shell elements (stiffening plates),
- Beam elements (rigid bars and guide rails),
- Truss elements (elastic tendons),
- Connectors (stiff tendons, retractors, sliding connections).

In all, the numerical model (illustrated in Fig. 10) is composed of 13,811 finite elements and 13,347 nodes. The temperature dependency of the gas behavior is included in the analysis. The prepared numerical model allows for simulation of the helium inflation (and deflation) into the each chamber independently.

The mission scenario is defined by the following steps:

Step-1: Preparing to start; in the initial configuration of the aerostat, all elastic tendons are prestressed to the level of σ_0, and then helium is partially removed (proportionally from all chambers) until the starting helium mass of m_{h2} is achieved; the temperature T_0 at the ground level is applied;

Step-2: Applying the compensating pressure load $p_e(h_2)$ and gas temperature from T_0 to T_2 caused by the altitude change of the aerostat from ground level h_0 to level of h_2;

Step-3: Removing gas at the altitude of h_2 (helium of mass m_{h1} remains);

Step-4: Aerostat descend to the altitude of h_1 (change the gas temperature from T_2 to T_1 and updating the compensating pressure load from $p_e(h_2)$ to $p_e(h_1)$);

Step-5: Fast helium removing at the altitude of h_1 (helium of mass $m_h^I(0)$ remains); the intermediate altitude of h_s is discussed in the next subsection;

Step-6: Aerostats descend to the ground level (change of the gas temperature from T_1 to T_0 and updating the compensating pressure load from $p_e(h_1)$ to $p_e(0)$).

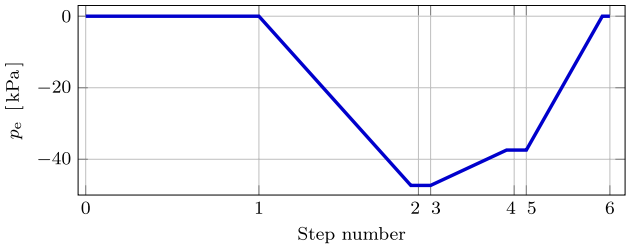

Fig. 11 Compensating load acting on the envelope induced by the decrease of the atmospheric pressure

Since the analysis covers processes conducted on the deployed state of the aerostat, the slidable joints are not activated and they work as pinned-connections. Similarly, retractors, are unlocked allowing the stiff tendons to change their lengths during ascending until they reach elongation of 15%. When this level is achieved, the retractors are switched into the locked state.

Figure 11 shows the applied compensating pressure load p_e caused by the altitude change scenario: h_0–h_2–h_1–h_0. Simultaneously, in the same fashion the temperature load for helium is applied, namely: T_0–T_2–T_1–T_0.

The crucial steps of the aerostat mission, as far as the envelope integrity is concerned, are Step-1 and Step-2 which are shown in the first two rows in Fig. 12. The highest equivalent von Mises stress (50 MPa) in the membrane (close to stiffening plates) is obtained at the end of Step-2 (altitude h_2, see Fig. 12b), however, in some of stiffening plates (neighboring to diaphragms), connected by means of rigid bars, the equivalent von Mises stress reaches 65 MPa. The maximum volume of the aerostat is reached at the end of Step-2 (the altitude h_2, $V_{max} = 24.01\,m^3$).

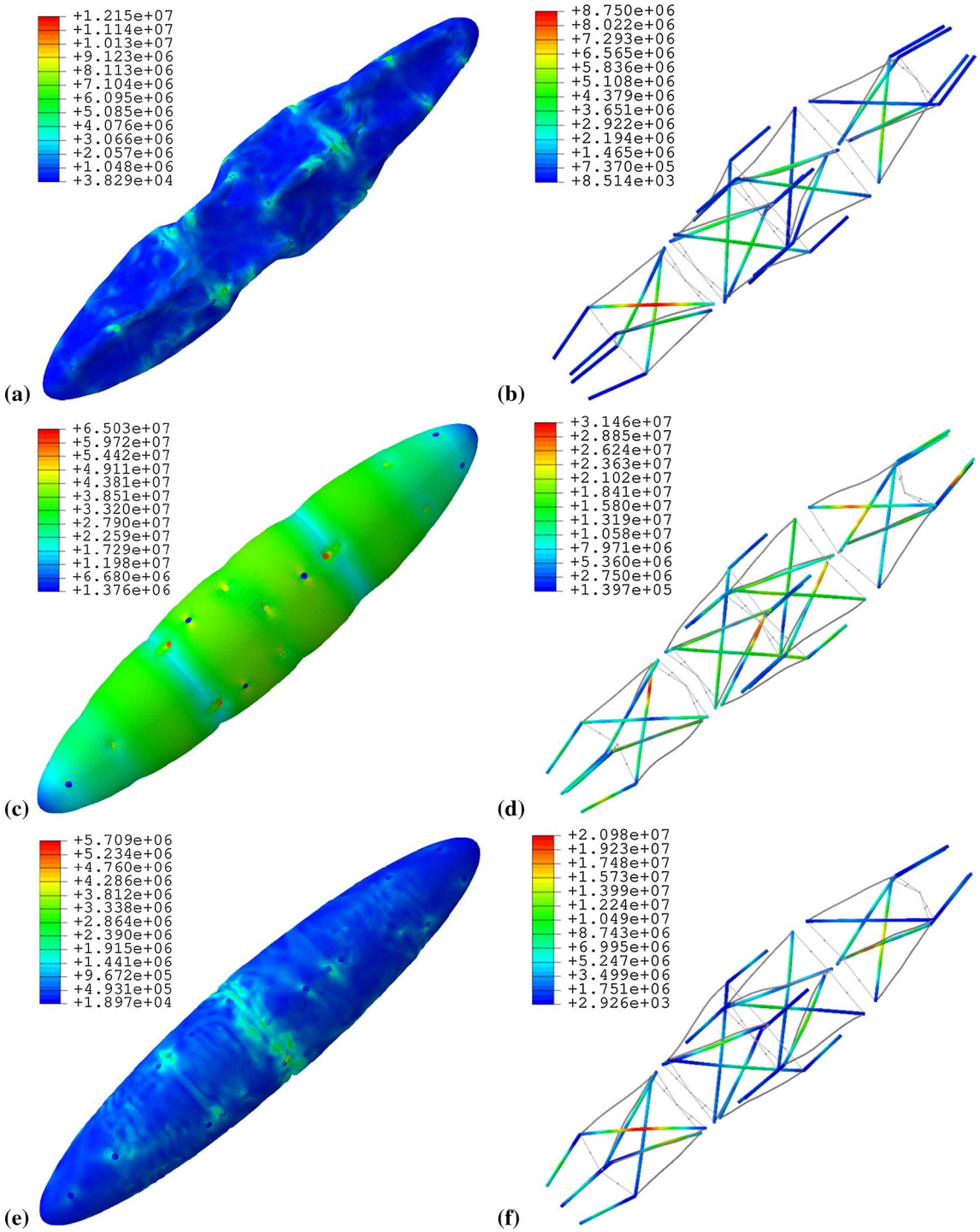

Fig. 12 Equivalent von Mises stresses (in pascals) in the aerostat membrane and internal structure: **a** and **b** at the end of Step-1; **c** and **d** at the end of Step-2; **e** and **f** at the end of Step-4

Table 3 Comparison of selected parameters for tendons shortening scenarios Step-5a to Step-5c

Parameter		Step-5a	Step-5b	Step-5c
Shortened tendons in sections		S1–S8	S3–S6	S1–S3 and S6–S8
Tendon reductions [%]		34.4	28.8	34.2
Δp [Pa]	Middle chamber	41.5	67.0	31.9
	Lateral chamber*	33.2	10.4	40.6
Force [N]	Section S1	62–71	48–51	67–88
	Section S2	53–68	≈ 0	55–66
	Section S3	58–61	136–158	54–73
	Section S4	63–72	86–100	28–31

*averaged from two lateral chambers

Based on this analysis, the volumetric stiffness coefficient k can be determined ($V > V_0$) using the relationship:

$$k = \frac{\Delta p}{\Delta V} V_0. \tag{22}$$

On the other hand, for the internal supporting structure the most crucial phase is Step-1 shown in Fig. 12b. In Step-1, the rigid bars tend to buckling when helium is being removed and the slidable joints are blocked. Further deflation without the slidable joints activation would lead to excessive stresses with possible structural damages. The right column in Fig. 12 presents equivalent von Mises stresses for the bars and guide rails (both of a beam type) of the supporting structure. The highest equivalent von Mises stresses reach almost 10 MPa and just over 31 MPa in members in the middle section in Step-1 and Step-2, respectively. In Step-1, the stiff tendons (designed to be tensioned in the operating state) are in loosened state. Longitudinal stresses in elastic tendons oscillate about initial stress level σ_0 (due to the low value of the Young modulus) and slightly decrease in the next steps. The elongation of stiff tendons does not exceed 15% at Step-2 when, thus the retractors are not locked (the equivalent von Mises stresses for the tendons are not shown in Fig. 12).

4.3 Adaptive morphing for altitude control of aerostats

The supporting structure is designed for a control of the aerostat altitude without changing of helium mass. Such strategy can be utilized for a temporary decrease of the aerostat altitude in a limited extent to the level of h_s which allows for carrying out service work (e.g., battery replacement or helium refilling).

If descending is required, a change of the aerostat volume is performed by selective shortening of the tendons at the end of each tensegrity section using remotely controlled electric motors. This means, that the final internal structure configuration necessary to achieve the required aerostat volume is not unique because different combinations of changing the lengths of tendons located at each end of tensegrity sections are possible. However, an optimization task can be used to determine the appropriate length of the tendons, e.g., with the criterion of minimizing the amount of energy required to change the aerostat position. Let us consider the aerostat altitude change from h_1 (at the end Step-4) into the service level of h_s using three different configurations of tendons:

Step-5a: Uniform shortening of all stiff tendons (sections S1–S8, cf. Fig. 10),
Step-5b: Uniform shortening of stiff tendons in the middle chamber (sections S3–S6),
Step-5c: Uniform shortening of stiff tendons in the sections S1–S3 and S6–S8.

Whereas the stiff tendons are shortened, both the aerostat volume and altitude are decreasing. The required volume V_s, required to achieve the planned altitude, can be determined using the static condition $Q_b = Q_g$ (cf. Eq. (4)), which yields

$$V_s(h_s) = \frac{m_t}{\rho_a(h_s)}. \tag{23}$$

The resulting aerostat configurations determined for Step-5a to Step-5c are shown in Fig. 13. For those cases the internal overpressures in the aerostat chambers are summarized in Table 3. The most varied value of Δp is obtained for squeezing the middle chamber (Step-5b) which results the highest axial forces in the tendons in the section S3 and S6. Utilizing all tendons (Step-5a) for the volume change involves their length reduction by 34.4% and for Step-5b and Step-5c the tendons are shortened by 28.8% and 34.2%, respectively (see Table 3).

The Ansys Fluent package was also used for an air flow evaluation of the aerostat shapes determined in Step-5a to Step-5c. The variation of the coefficient c_x and drag force Q_d in terms of aerostat velocity v up to 5 m/s are presented in Fig. 14 with dual axes. These values of the coefficient

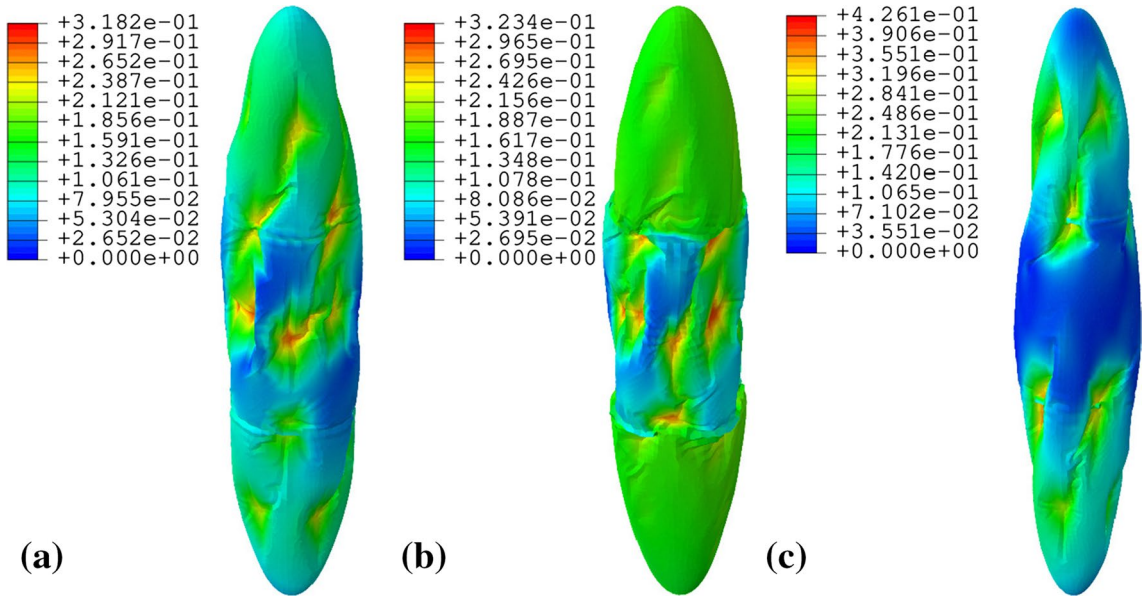

Fig. 13 Aerostat configurations (total displacements [m]) obtained for scenario: **a** Step-5a, **b** Step-5b and **c** Step-5c

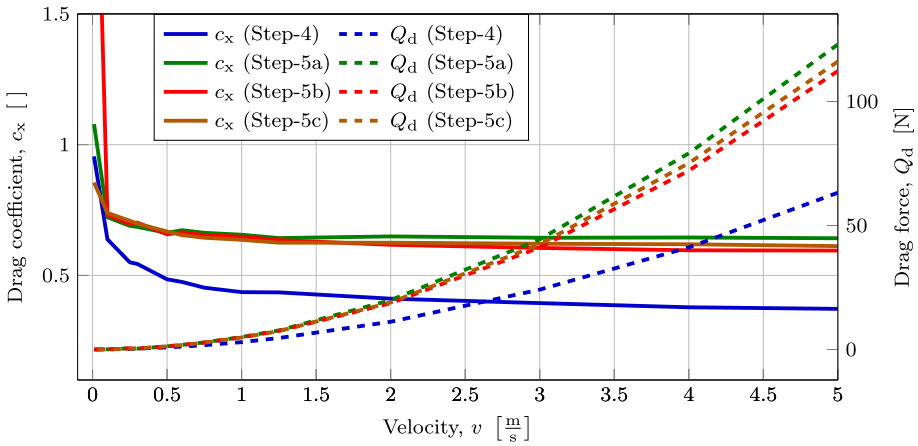

Fig. 14 Determined dependencies of the drag coefficient c_x and the drag force Q_d for selected aerostat shapes

c_x can be also used in the Matlab/Simulink model. On the left side is the reference to the drag coefficient c_x, while on the right one is the drag force Q_d. In fact, for aerostat shape configurations in Step-5a to Step-5c, the both quantities the drag coefficient c_x and drag force Q_d almost overlap each other especially in low wind speed regime and clearly differ from the results obtained for Step-4. The path lines of the air flows for the aerostat configurations Step-5a to Step-5c are shown in Fig. 15.

Figure 16 presents the summary of the results of variant I and variant II control and shows the variations of the aerostat volume $V(h)$ during its ascending and descending. The climbing path is outlined by the continuous red line and lies above the blue curve, which was computed using Eq. (23) in order to determine the static equilibrium positions. In contrast to climbing path, there are two variants of descending paths I and II which are placed below the static curve and drawn with dashed lines.

The variant I representing the exclusive helium mass control is marked with dashed red line. In the variant II between the altitudes h_2 and h_1 when helium mass control is used the results are the same as in the variant I. Changes between the altitudes h_1 and h_s, when exclusive tendons control is used, are marked with green dashed line. The last section of variant II below the altitude h_s is marked with brown dashed line. One can observe the discrepancy between red and green or brown dashed lines resulting from the assumption of different descent rates in the variant I and II. This relationship shows that for the lower descent velocities, the descent paths will be closer to the static equilibrium line for a given aerostat. However, it should be noted that also possibility of obtaining higher

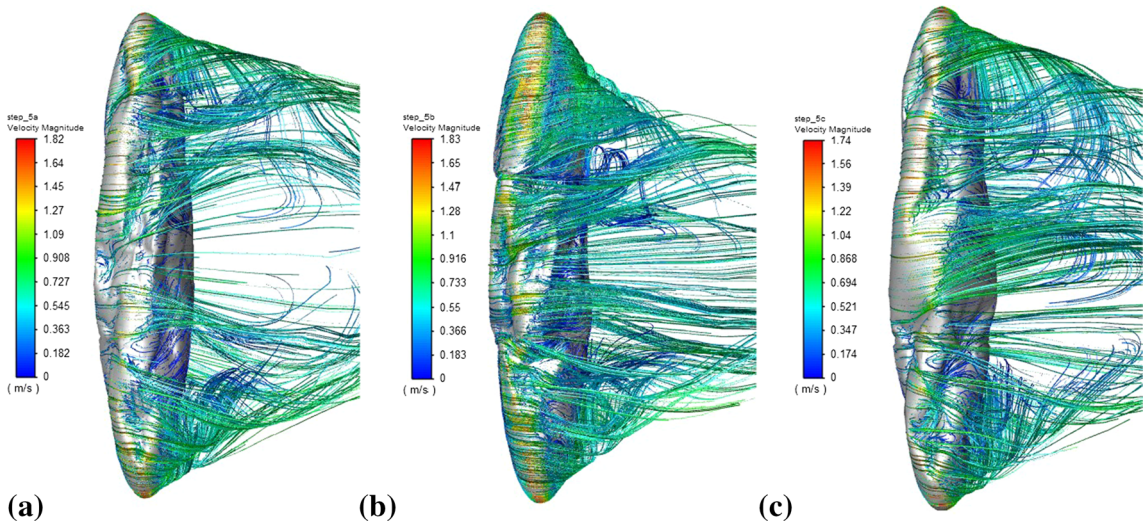

Fig. 15 Path lines of the air flows computed for the vertical aerostat velocity of 1 m /s for scenario: **a** Step-5a, **b** Step-5b and **c** Step-5c

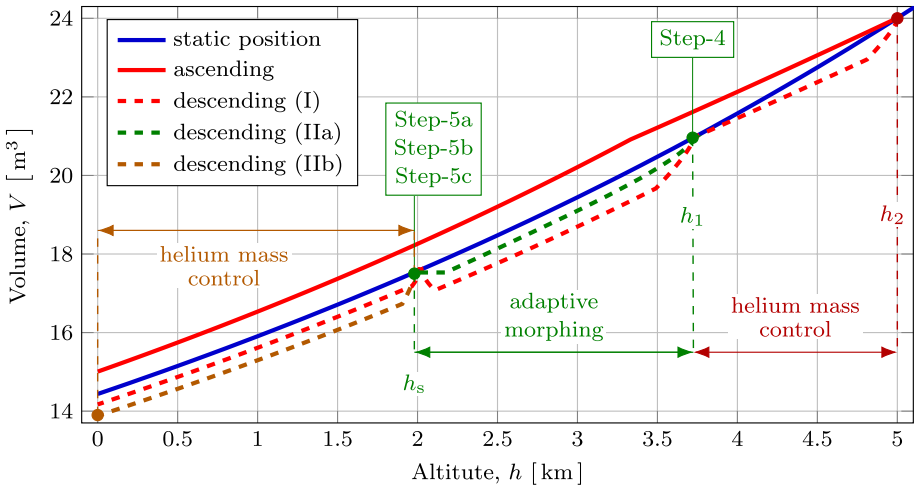

Fig. 16 Aerostat volume variation during climbing and descending paths

speeds is limited by the strength of the envelope and internal structure of the aerostat.

4.4 The control scheme of the adaptive morphing

A general scheme of the control strategy for adaptive morphing is shown in Fig. 17. The input data for the morphing are actual position of the aerostat, actual values of the control parameters (m_h and ε_t), imposed constraints and data concerning required new position of the aerostat. The optimization of the control parameters of the adaptive morphing can utilize the sum of two components:

- Energy needed to change vertical position of the aerostat, and
- Energy needed to change its horizontal position.

The component describing the change of vertical position takes into account the work done by the drag force (which depends on obtained coefficient c_x in lateral direction), the work required for helium compression (which depends on submitted helium mass $m_h(t)$) and the work required for tendons elongation change (which depends on tendons shortening $\varepsilon_t(t)$). In turn, the component describing the change of horizontal position takes into account the propulsion work and the work of wind thrust (which both depend on coefficient c_x in axial direction) as well as mentioned previously work of helium compression and work of tendons elongation (which depend on $m_h(t)$ and $\varepsilon_t(t)$, respectively). In the case of joint vertical and horizontal movement of the aerostat, the objective function of the dynamic optimization problem is the sum of mentioned components with weighting coefficients (w_1 and w_2). The result of solved minimization problem are the functions describing the change of helium mass

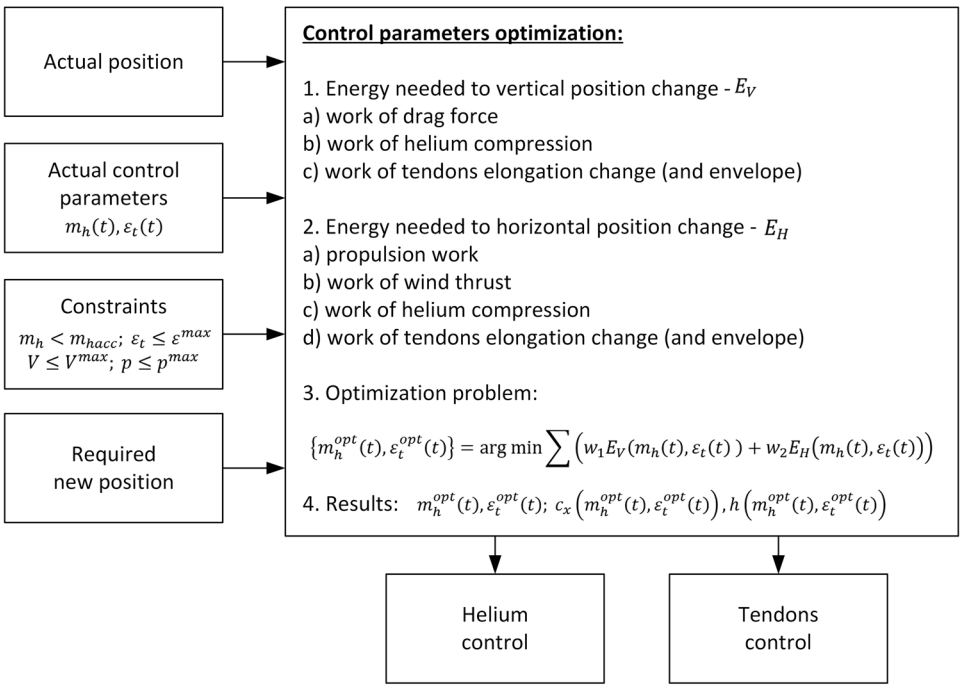

Fig. 17 The control scheme of the adaptive morphing

and tendons shortening in time, $m_h^{opt}(t)$ and $\varepsilon_t^{opt}(t)$, required for assumed aerostat repositioning and satisfying the optimality criterium and constraints. Based on these functions, the decision concerning application of helium mass control, tendons control or combination of both methods can be made and the optimal control can be applied.

5 Conclusions

In conclusion, the concept of tensegrity-type ultra-light rod-cable structures applicable as self-deployable reinforcement for helium aerostats seems to be a promising solution which enables energy efficient control of the airship vertical motion. The self-deployable concept of the supporting structure can be especially interesting in the case of need for prompt, precisely designed action (location and timing of modifiable scenario) for monitoring of important, spreaded event. This can be achieved by folding the aerostat structure (1D transport configuration) then fast lifting it utilizing an airplane or a launch rocket and finally unfolding the structure (3D operational configuration) at the planned altitude. This type of the structure enables easy to use adaptive morphing for control the aerostat volume and shape. The divided internal space of the aerostat can be also used for the horizontal stabilization by control of the helium mass distribution between chambers.

Important advantage of the proposed Adaptive Helium Aerostat with the Self-Deployable Tensegrity concept (AHA-SDT) is possibility of changing volume and shape of the airship by applying concentrated forces, with semi-active, low-energy-consuming smart control systems. These issues will be investigated in the following papers, opening development option for the adaptive, hybrid system (satellite and stratospheric aerostats) of the environment observation.

Although the results obtained and presented are promising, many further issues need to be solved. The next research will be devoted to various options of the aerostat operations, e.g., rapid elevation to the starting altitude h_1. On the other hand, the techniques for experimental verifications (the airship is under construction) of the discussed numerical modeling are to be investigated. Then, the strategies of adaptive morphing, controlling V-Mobility of the AHA-SDT aerostat, in case of various missions to be performed, will be also discussed. Finally, the problems of H-Stabilization (horizontal stabilization), making use of ballonets separated with diaphragms, and H-Mobility (horizontal mobility) will be also addressed.

The following papers of the authors will be aimed at formulating a novel and complete approach to the concept of tensegrity-based helium-filled aerostats, designed for specified missions, to be performed in determined location and time. This approach assumes possibility of:

– Self-deployment of the airship structure from a compact 1D form (fitted into a tube for the transport phase) to the final, functional 3D form (when the operational level h_1 is reached);

(a) (b)

Fig. 18 Two prototypes of the tethered aerostats designed for an aerial monitoring: **a** MK-7 (7 m long) and **b** MK-10 (10 m long)

- Tensegrity-based aerostat design allowing to perform mission in the operational altitude from h_1 to h_2 which requires significantly smaller growth of its volume than traditional, autonomous elevation from the ground level $h_0 = 0$ to the operational altitude;
- Self-adaptivity of the aerostat volume and shape, which allows to reach the altitudes and to achieve stable operational position which results in significant cost and weight saving.

Currently, the authors are testing two prototypes of the tethered aerostats, shown in Fig. 18, designed at the Institute of Fundamental Technological Research of the Polish Academy of Sciences for an aerial monitoring. Based on the obtained results, another aerostat prototype with the presented tensegrity structure is currently being developed.

Funding The authors acknowledge the support of the National Centre for Research and Development and the National Science Centre, Poland, granted in the framework of the TANGO 4 programme (project TANGO-IV-C/0001/2019-00) and the project DEC-2017/25/B/ST8/01800 of the National Science Centre, Poland.

Declarations

Conflict of interest The authors declare no conflict of interest.

Ethical approval This article does not contain any studies with human participants or animals performed by any of the authors.

Informed consent Informed consent was obtained from all individual participants included in the study.

References

1. Brayan T, Rava G. British Airships 1905–30. New York: Osprey Publishing, May 1, 2009. 48 pp. isbn: 184603387X. URL: https://www.ebook.de/de/product/8088559/british_airships_1905_30.html.
2. Ege, L. Baloons and Airships. London: Blandford Press, 1974. URL: https://www.ebook.de/de/product/8088559/british_airships_1905_30.html.
3. Chaplain CT et al. Future aerostat and airship investment decisions drive oversight and coordination needs. Tech. rep. GAO-13-81. United States Government Accountability Office, 2012. URL: https://www.gao.gov/assets/650/649661.pdf.
4. Rees JJS (ed) Recent development efforts for military airships. Tech. rep. The Congress of the United States, Congressional Budget Office, 2011. URL: https://fas.org/irp/program/collect/cbo-airship.pdf.
5. Saleh S, He W. New design simulation for a high-altitude dual-balloon system to extend lifetime and improve floating performance. Chin J Aeronaut. 2018;31(5):1109–18. https://doi.org/10.1016/j.cja.2018.03.009.
6. D'Oliveira FA, de Melo FCL, Devezas TC. High-altitude platforms–present situation and technology trends. J Aerosp Technol Manag. 2016;8(3):249–62. https://doi.org/10.5028/jatm.v8i3.699.
7. Smith S et al. "HiSentinel80: Flight of a high altitude airship". 11th AIAA Aviation Technology, Integration, and Operations (ATIO) Conference, including the AIAA Balloon Systems Conference and 19th AIAA Lighter-Than-Air Technology Conference. 2011. https://doi.org/10.2514/6.2011-6973.
8. Jiang Y, Lv M, Li J. Station-keeping control design of double balloon system based on horizontal region constraints. Aerosp Sci Technol. 2020;100: 105792. https://doi.org/10.1016/j.ast.2020.105792.
9. Liu J-M, Lu C-J, Xue L-P. Investigation of airship aeroelasticity using fluid-structure interaction. J Hydrodyn. 2008;20(2):164–71. https://doi.org/10.1016/s1001-6058(08)60042-6.
10. Zhao S, et al. Change rules of a stratospheric airship's envelope shape during ascent process. Chin J Aeronaut. 2017;30(2):752–8. https://doi.org/10.1016/j.cja.2017.02.017.
11. Liao J, et al. A passive approach for adjusting the diurnal temperature difference of the envelope of stratospheric light aerostat. Aerosp Sci Technol. 2019;91:494–507. https://doi.org/10.1016/j.ast.2019.05.042.
12. Hu Y, et al. Modal behaviors and influencing factors analysis of inflated membrane structures. Eng Struct. 2017;132:413–27. https://doi.org/10.1016/j.engstruct.2016.11.037.
13. Szyszkowski W, Glockner PG. Spherical membranes subjected to vertical concentrated loads: an experimental study. Eng Struct. 1987;9(3):183–92. https://doi.org/10.1016/0141-0296(87)90014-9.
14. Wang S, et al. Nonlinear 3D numerical computations for the square membrane versus experimental data. Eng Struct. 2011;33(5):1828–37. https://doi.org/10.1016/j.engstruct.2011.02.023.

15. Li Y, Nahon M, Sharf I. Dynamics modeling of flexible airships. 48th AIAA/ASME/ ASCE/AHS/ASC Structures, Structural Dynamics, and Materials Conference. American Institute of Aeronautics and Astronautics, 2007, p 10. https://doi.org/10.2514/6.2007-2212.
16. Li Y, Nahon M. Modeling and simulation of airship dynamics. J Guid Control Dyn. 2007;30(6):1691–700. https://doi.org/10.2514/1.29061.
17. Zhao Y, Garrard W, Mueller J. Benefits of trajectory optimization in airship flights. AIAA 3rd "Unmanned Unlimited" Technical Conference, Workshop and Exhibit. American Institute of Aeronautics and Astronautics, 2004; 591–604. https://doi.org/10.2514/6.2004-6527.
18. Zuo Z, et al. Three-dimensional path-following backstepping control for an underactuated stratospheric airship. IEEE Trans Aerosp Electron Syst. 2019;55(3):1483–97. https://doi.org/10.1109/taes.2018.2873054.
19. Kahale E, Garcia PC, Bestaoui Y. Autonomous path tracking of a kinematic airship in presence of unknown gust. J Intell Robot Syst. 2012;69(1–4):431–46. https://doi.org/10.1007/s10846-012-9709-2.
20. Mueller JB, Zhao YJ, Garrard WL. Optimal ascent trajectories for stratospheric airships using wind energy. J Guid Control Dyn. 2009;32(4):1232–45. https://doi.org/10.2514/1.41270.
21. Yongmei W et al. Trajectory tracking of a high altitude unmanned airship based on adaptive feedback linearization. 2011 International Conference on Mechatronic Science, Electric Engineering and Computer (MEC). IEEE, 2011; 2257–2261. https://doi.org/10.1109/mec.2011.6025942.
22. Zheng Z, Liu L, Zhu M. Integrated guidance and control path following and dynamic control allocation for a stratospheric airship with redundant control systems. Proceedings of the Institution of Mechanical Engineers, Part G: Journal of Aerospace Engineering. 2016;230(10):1813–26. https://doi.org/10.1177/0954410015613738.
23. Oliveira MC, Skelton RE. Tensegrity systems. Springer US, 2009. https://doi.org/10.1007/978-0-387-74242-7.
24. de Oliveira MC, Wroldsen AS. Dynamics of tensegrity systems. Efficient modeling and control of large-scale systems. Springer US, 2010; 73–88. https://doi.org/10.1007/978-1-4419-5757-3_3.
25. Williamson D, Skelton RE. General class of tensegrity structures: topology and prestress equilibrium analysis. J Guid Control Dyn. 2003;26(5):685–94. https://doi.org/10.2514/2.5119.
26. Snelson K. Snelson on the tensegrity invention. Int J Space Struct. 1996;11(1–2):43–8. https://doi.org/10.1177/026635119601-207.
27. Peng H, et al. Symplectic instantaneous optimal control of deployable structures driven by sliding cable actuators. J Guid Control Dyn. 2020;43(6):1114–28. https://doi.org/10.2514/1.g004872.
28. Arcaro V, Adeli H. Form-finding and analysis of hyperelastic tensegrity structures using unconstrained nonlinear programming. Eng Struct. 2019;191:439–46. https://doi.org/10.1016/j.engstruct.2019.04.060.
29. Phocas MC, Christoforou EG, Dimitriou P. Kinematics and control approach for deployable and reconfigurable rigid bar linkage structures. Eng Struct. 2020;208: 110310. https://doi.org/10.1016/j.engstruct.2020.110310.
30. Korkmaz S, Ali NBH, Smith IF. Determining control strategies for damage tolerance of an active tensegrity structure. Eng Struct. 2011;33(6):1930–9. https://doi.org/10.1016/j.engstruct.2011.02.031.
31. Feng X, Miah MS, Ou Y. Dynamic behavior and vibration mitigation of a spatial tensegrity beam. Eng Struct. 2018;171:1007–16. https://doi.org/10.1016/j.engstruct.2018.01.045.
32. Veuve N, Safaei SD, Smith IF. Active control for mid-span connection of a deployable tensegrity footbridge. Eng Struct. 2016;112:245–55. https://doi.org/10.1016/j.engstruct.2016.01.011.
33. Knap L, et al. Strategies for reduction of energy consumption during ascending and descending process of modern telescopic HAPS aerostats. Bull Pol Acad Sci Tech Sci. 2020;68(1):155–68. https://doi.org/10.24425/bpasts.2020.131833
34. Kumar BS, et al. Mechanical properties of ANTRIX balloon film and fabrication of single cap large volume balloons. Adv Space Res. 2008;42(10):1691–7. https://doi.org/10.1016/j.asr.2008.03.030.